BIOSYSTEMS ENGINEERING 164 (2017) 171–180

Available online at www.sciencedirect.com

ScienceDirect

journal homepage: www.elsevier.com/locate/issn/15375110

Research Paper

Semi-automated, machine vision based maize kernel counting on the ear

Tony E. Grift [a,*], Wei Zhao [a], Md Abdul Momin [a], Yu Zhang [b], Martin O. Bohn [c]

[a] Department of Agricultural and Biological Engineering, University of Illinois, Urbana, IL 61801, USA
[b] Department of Agricultural and Biosystems Engineering, North Dakota State University, Fargo, ND 58102, USA
[c] Department of Crop Sciences, University of Illinois, Urbana, IL 61801, USA

ARTICLE INFO

Article history:
Received 21 December 2016
Received in revised form
11 October 2017
Accepted 26 October 2017

Keywords:
Plant phenotyping
Image processing
Corn

In synchrony with the overall trend toward automation in plant phenotyping, two semi-automatic machine vision methods were devised targeted at counting maize kernels directly on de-husked ears. The ears represented row morphologies ranging from straight to curved, they featured missing kernels, underdeveloped kernels, and broken kernels, but displayed no disease or mould.

The first method mimicked a common manual field method of estimating the total ear kernel count, based on counting the number of rows and multiplication by the number of kernels per row. Similarly, in this paper, the operator manually counted the number of rows, and also manually counted the number of kernels in a row image within an (operator determined) quasi-cylindrical mid-section of the ear. The total ear kernel count was then estimated by multiplying the number of rows by the number of kernels per row, yielding full ear extrapolation by multiplication by the ratio between the total ear length and the length of the quasi-cylindrical mid-section. This full ear image based approach achieved a kernel counting error ranging from −7.67% (under-count) to +8.60% (multi-count) among 23 maize ears.

The second method only observed a fixed quasi-cylindrical mid-section of the ear. Image frames were acquired of each individual row of kernels located in the quasi-cylindrical mid-section, yielding kernel maps. Among 12 maize ears, the kernel missing error ranged from 0 to 4.24% and the multi-count error ranged from 0 to 1.92%. In total, 41 existing kernels were missed and 25 kernels were multi-counted among 2713 kernels counted.

1. Introduction

The objective and consistent gathering of phenotypical information from maize and other crops is an important, yet deficient topic in maize breeding programs. Machine vision is well suited to, in a high-throughput manner, quantify plant phenomena that are typically scored by human evaluators (Shyu et al., 2007). The machine vision approach also has the

* Corresponding author.
E-mail address: grift@illinois.edu (T.E. Grift).
https://doi.org/10.1016/j.biosystemseng.2017.10.010
1537-5110/

advantage of creating digital records of the ears allowing revisiting and reuse when new analysis algorithms become available. Imaging techniques have shown capable of quantifying elusive traits such as the complexity of maize roots, which was expressed in the Fractal Dimension (Bohn, Novais, Fonseca, Tuberosa, & Grift, 2006) as well as Root Top Angle (Grift, Novais, & Bohn, 2011). In the area of maize kernel analysis, a machine vision system was developed to characterise the shapes of kernels as either convex, smooth dent or non-smooth dent shapes (Ni, Paulsen, & Reid, 1997). In addition, an image processing method including a watershed procedure was developed to count maize kernels after shelling (Severini, Borrás, & Cirilo, 2011). Finally, to count the number of maize ear rows,[1] a machine vision method was developed (Han, Li, Zhang, & Zhao, 2010). One patent application regarding the use of machine vision to analyse maize ears was filed (Hausmann, Abadie, Cooper, Lafitte, & Schussler, 2011).

A common manual procedure for counting kernels on a maize ear relies on multiplying the number of kernel rows, which typically range from 12 to 18, by the number of kernels per row. The latter is difficult to count, since an ear contains a tapered base and tip where the number of rows eventually reduces to nil. This procedure inherently ignores the tapering effect, since essentially, an extrapolation is performed from the section where the number of rows is constant (termed the quasi-cylindrical mid-section in this paper) to the total ear kernel count. As a digital equivalent of this method, in this research, a machine vision approach was taken in which the operator counts the number of rows, and indicates the quasi-cylindrical mid-section using a mouse on a screen. Then the software multiplies the number of rows by the number of kernels per row in the quasi-cylindrical mid-section, and extrapolates to the total ear kernel count by further multiplication by the ratio of the total ear length, and the length of the quasi-cylindrical mid-section.

The second method also includes counting kernels, but it only observed the quasi-cylindrical mid-section which is fixed by the camera parameters and the imaging geometry. This method obviously does not yield a total ear kernel count, but it does yield a kernel density (number of kernels per area), and, more importantly, it yields a map of all kernels in the quasi-cylindrical mid-section. This allows for the calculation of several kernel properties such as area and centre of mass (these were in fact used to detect multi-counting) as well as circumference, major and minor axes, orientation, eccentricity, equivalent diameter, and perimeter using MatLab's "regionprops" function. The fact that this approach yields a number of morphological parameters for each kernel is of importance to maize breeders who are determining which genes are involved in creating the morphological parameters observed through quantitative trait loci (QTL) mapping.

The level of automation was kept such that the system would remain relatively inexpensive, and yet have a reasonable throughput of approximately one ear per minute.

[1] Since in this research the ear is always presented vertically, the term "kernel column" would be more appropriate, but to keep terminology consistent with other publications, the term "kernel row" will be used throughout.

The objective of this research was to develop and evaluate the performance of two kernel counting methods, being 1) an estimator of the total ear kernel count through extrapolation of manually counted kernels in a quasi-cylindrical mid-section selected by the operator, and 2) an estimator of the number of kernels in a fixed quasi-cylindrical mid-section of a maize ear, including a procedure enabling the creation of kernel maps with ample morphological kernel feature information.

2. Materials and methods

Maize ears were collected from a crop grown at the Agricultural Engineering farm of the University of Illinois (lat: 40.072601, lon: -88.210139). The ears were produced through a breeding program where various hybrids were grown. They were chosen to reflect a number of ear phenotypes from simple, implying straight rows of kernels, to complex, implying helix shaped rows of kernels. None of the ears was affected by fungal disease or mould. The ears were de-husked in the field, and transported carefully to a laboratory to avoid losing kernels in the process. Before ear imaging, any remaining silk strands on the ear were brushed off to avoid potential "bridging" of kernels after segmentation. A 6.35 mm hole was drilled in each ear using a drill press, allowing vertical presentation of the ear in an imaging arrangement.

2.1. *Imaging arrangement*

The images of the maize ears were acquired in a "soft box" as shown in Fig. 1. To ensure images featuring abundant detail, proper lighting is paramount. Therefore, the soft box was fitted with a light reflector with a diameter of 200 mm, (Smith Victor Q80, Adorama Camera, Inc., New York, NY) containing a 300 Watt DYS type halogen bulb. The light from the bulb was passed through a diffusing layer, consisting of a transparent sheet of High Density Polyethylene (HDPE) material with a thickness of 3.175 mm, before entering the imaging cube. This method, in combination with non-reflective walls, yielded a high-quality diffused lighting scene. The soft box was built from HDPE panels, a material typically used to produce cutting boards for domestic use. It has good light reflective properties, and withstands water and contamination very well. In fact, it adheres poorly to any chemical, including bonding agents, therefore the box was constructed using bolts and fasteners. The HDPE panels had a thickness of 19 mm, and they formed a cubic imaging cavity sized at 590.55 mm. To increase the contrast for ear imaging, a black background was installed made from non-reflective cardboard (not shown in Fig. 1). During image acquisition, the ear was placed on a spike that was rotated by a uni-polar 12 V DC 600 mA stepper motor (part no. 162027, Jameco, Belmont, CA), featuring a step angle of 0.9° in half step mode, allowing up to 400 unique images per revolution. The drive section of the soft box contains the stepper motor, a coupler that connects the mounting spike to the stepper motor, a stepper motor controller board with a serial interface (model STP100, Pontech, Rancho Cucamonga, CA), and a 12 V, 60 W power supply (part no. 2105308, Jameco, Belmont, CA). Two identical colour cameras (Unibrain, model

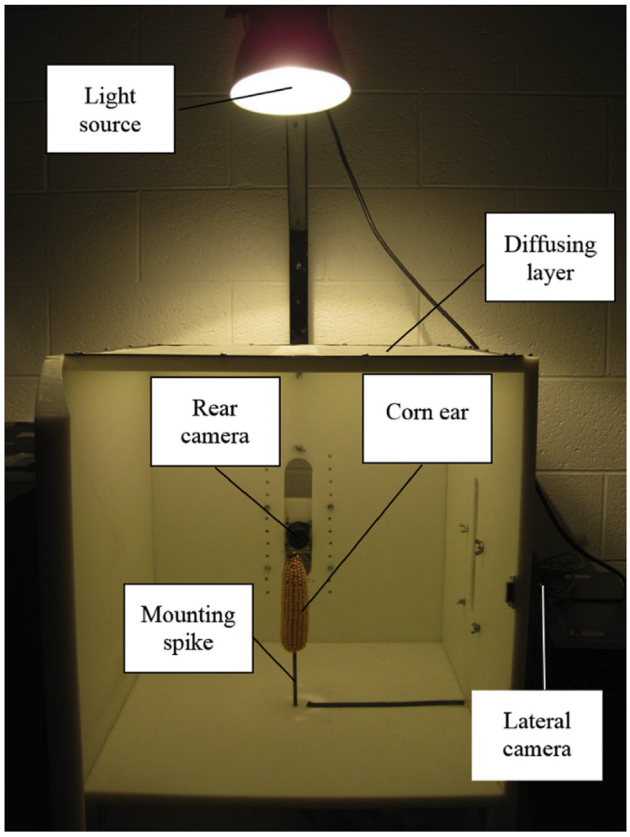

Fig. 1 – A "soft box" was used which provided a highly diffused lighting scene by channelling light from a point source through a diffusing layer. The box was made from High Density Polyethylene (HDPE) material, which has good reflective properties and rejects water and contamination well. The light source was a 300 W halogen photography bulb. The camera in the rear captured the whole ear, whereas the lateral camera captured a constant size quasi-cylindrical mid-section of the ear. For imaging the ear was mounted on a spike that was automatically rotated so as to capture each row of kernels frontally by the side camera.

701c) with a resolution of 1280 × 960 pixels were fitted in the soft box. A lateral camera was mounted in the side panel to provide a landscape mode image of the ear's fixed quasi-cylindrical mid-section, therefore a lens with a focal length of 16 mm was fitted (Fujinon, model 630079). A rear camera was mounted in the back panel of the soft box, and it was fitted with a 6 mm focal length lens (Pentax, model C60607KP) to provide a portrait mode image of the complete ear for total ear kernel counting. The cameras were controlled by a program written in MatLab®, using an IEEE 1394 (FireWire®) interface. MatLab® was also used to control the stepper motor and for analysis of the imagery.

2.2. *Total ear kernel counting*

As a digital counterpart of the traditional in-field manual total ear kernel counting method, images of full ears were acquired using the rear camera fitted in the imaging box (Fig. 1). In advance, the operator counted the number of ear rows present, and then placed the ear on the spike in the imaging box. Subsequently, the rear camera acquired a portrait mode full ear image which was presented to the operator (Fig. 2). The

Fig. 2 – Example maize ear image used to estimate the total ear kernel count. Distance D2 represents the total ear length, whereas D1 is the distance chosen by the operator to represent the variable size quasi-cylindrical mid-section.

operator then marked the section considered the quasi-cylindrical mid-section of the ear (D1 in Fig. 2) and counted the number of kernels along a single row in this section. The total ear kernel count was calculated by multiplying the number of kernels counted along a single row in the quasi-cylindrical mid-section by the manually counted number of rows and by the ratio of the total ear length (D2) and the length of the quasi-cylindrical mid-section (D1). Both values D1 and D2 were obtained by mouse clicks on a computer screen. The expectation was that the method would be biased toward multi-counting since the tapered base and tip of the ear are treated as if they are part of the quasi-cylindrical mid-section, but this was found not to be the case.

2.3. *Kernel counting and mapping in the quasi-cylindrical mid-section of the ear*

The semi-automated counting of kernels in the quasi-cylindrical mid-section of the ear poses a far more difficult problem than the total ear kernel counting method, since it attempts to isolate, count, and evaluate each kernel in this section individually. The imaging parameters of the lateral camera were such that an area of approximately 10 cm in height was observed from the quasi-cylindrical mid-section of a typical ear, containing up to approximately 20 kernels per row. To create a kernel map of a maize ear, each kernel in the quasi-cylindrical mid-section must be presented frontally to the camera at least once. Therefore, the operator was asked to enter the number of rows on the ear (typically ranging from 12 to 18) and then to place the ear on the spike while one kernel row was presented approximately frontally to the lateral camera. Although MatLab® has the "imaqtool" feature, which provides a live camera view usable for real-time alignment, it was not needed in practice. Subsequently, the computer turned the ear through the number of degrees needed to frontally capture consecutive image frames of each kernel row, which was equal to 360° (represented by 400 pulses to the stepper motor) divided by the number of kernel rows. For example, if the ear had 17 rows, the rotational angle was 360/17 = 21.176°, which is equivalent to (400/360)*21.176 = 23.529 pulses to be sent to the stepper motor. This value has to be integer, therefore the real number of pulses was rounded off to 24, and therefore the stepper motor total turning angle was 367.2°, meaning that the first and last image would be near impossible to overlap. As an alternative, an extra rotation was applied and an extra image taken. In the example given, image

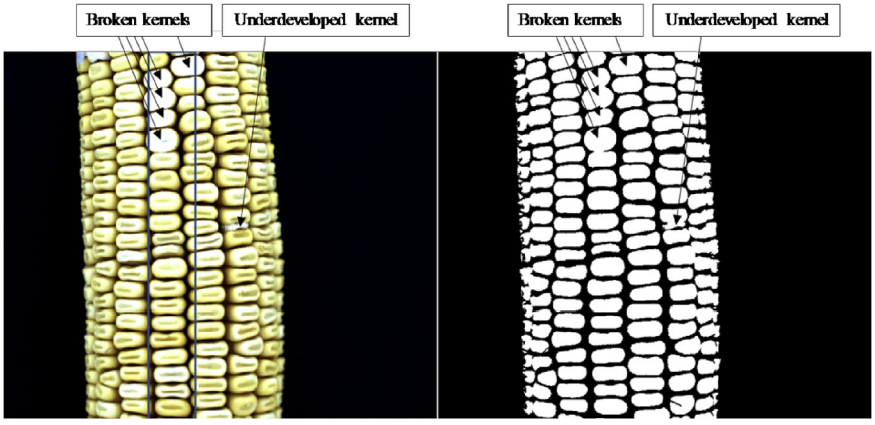

Fig. 3 – Left: Original colour image of a maize ear's quasi-cylindrical mid-section. The blue rectangle indicates the observation window in which kernels are evaluated for multi-counting. Right: Same image after thresholding using Otsu's method. Notice that the kernels are separable with this standard technique, unless they are either broken (presenting a flat face) or underdeveloped. Note that the kernel blobs in the right image were filled in with MatLab's "imfill" function. (For interpretation of the references to colour in this figure legend, the reader is referred to the web version of this article.)

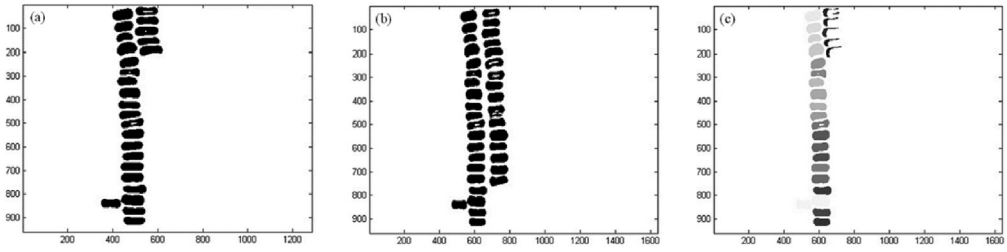

Fig. 4 – To prevent counting kernels more than once, subsequent image frames were compared. If a kernel was detected in the left frame, and again in the middle frame, overlap was detected with a logical AND function, which changes its overlapped area (see right frame, top 5 kernels). Since these kernels were observed previously, they should not be counted again. Accumulation of a set of multi-count corrected frames comprised a kernel map of the ear.

17 was thus overlapped with image 18 rather than image 1. The total throughput time to process a single maize ear was approximately 1 min. This estimate assumes that drilling of the hole and removal of silk strands was done simultaneously with imaging of a previous ear.

2.3.1. *Image analysis*

Figure 3 shows an image of the quasi-cylindrical mid-section of an ear. The left image shows the raw colour image, whereas the right image shows the same image after segmentation. For segmentation, the RGB colour image was read, then MatLab's function "graythresh" was called to obtain a global threshold value and subsequently MatLab's function "im2bw" was applied using the threshold value to obtain a binary image. As Fig. 3 shows, in the case of healthy kernels, this standard procedure using Otsu's method (Otsu, 1979) was able to separate kernels in the central rows, but in the case of broken, flat headed kernels and an underdeveloped kernel it caused "bridging" among these and neighbouring kernels. Bridging will cause two or more kernels to be counted as one, unless it is detected and compensated for. Note that the segmented kernels shown in the right hand image of Fig. 3 sometimes had holes that were filled in with MatLab's "imfill" function. After segmentation, a single erosion/dilation operation was applied to eliminate single pixel noise. Subsequently, MatLab's blob analysis tools were used to create a label image, after which MatLab's "regionprops" function was called, allowing measurement of several parameters of each blob (kernel) including the blob area and centre of mass. The latter two parameters were used in the counting process to determine whether a kernel was multi-counted.

2.3.2. *Detection of multi-counted kernels*

To count the kernels on a maize ear in the quasi-cylindrical mid-section, they all have to be detected and assigned one count per kernel. As is evident in Fig. 3, kernels located at the left and right edges of the ear present a projected area, as well as being occluded by other kernels, and only kernels in the central row inside the blue rectangular box are frontally observed. Therefore, an observation window was set to select

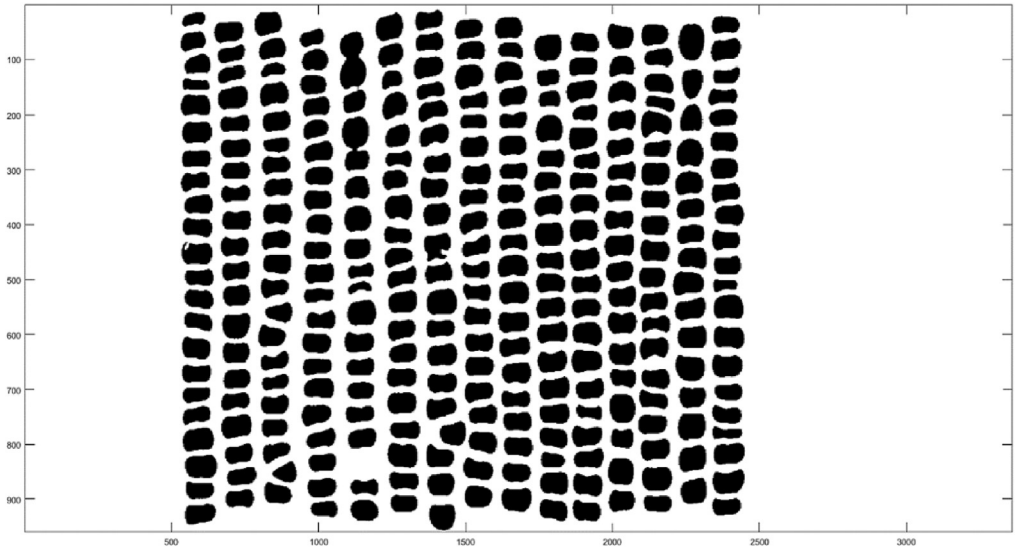

Fig. 5 – A kernel map is shown which can be used for counting kernels in the quasi-cylindrical mid-section but also to calculate various morphological parameters of individual kernels.

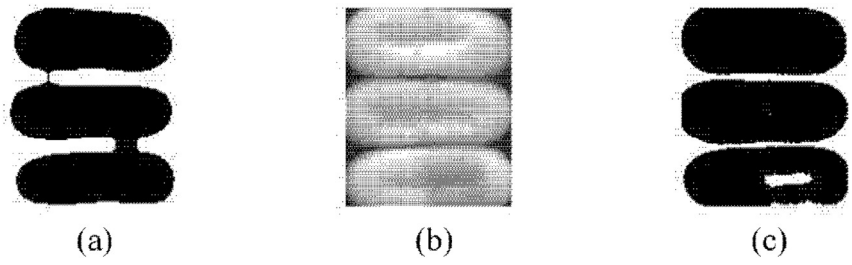

Fig. 6 – In some cases, Otsu's segmentation method failed to completely separate kernels, and left bridges among the kernels (a). Kernel groups affected by bridging were detected by area discrimination. The bridged kernels were traced back to the original grey scale image (b), and re-segmented with a local threshold value. Sometimes this caused holes in blobs (c) which were filled in with MatLab's "imfill" function.

kernels in the centre of the maize ear. The window width is a trade-off: when set too wide, many kernels would be multi-counted, and when set too narrow many existing kernels would remain uncounted. The window was placed symmetrically around the location of the spike on which the ear was pinned, and the window width was set to twice the shift distance in pixels between two consecutive image frames. Only kernels that had a centre of mass located inside the observation window were assumed frontally exposed. The observation window was the first level of preventing multi-counting of kernels, but it is not sufficient, since some kernels will be observed in more than one image frame. Therefore, a more advanced anti multi-counting method was developed as follows. Figure 4a shows a segmented image, where kernels from three rows are present in a single image. Note that row 1 contains 1 kernel, row 2 contains 20 kernels and row 3 contains 5 kernels. Figure 4b shows the accumulative image after a motor rotation to observe the adjacent kernel row. Note that now 17 kernels are present in row 3 (also note that the 10th kernel in row 3 contains an underdeveloped kernel). The problem here is that the top 5 kernels in the third row were also present in the third row of the previous frame (4a), and thus already counted: unless this effect is compensated for, they each would be counted twice. Figure 4c shows how this is prevented. All kernels in the right hand row in Fig. 4b are shifted to the left by the number of pixels that represent the horizontal shift per consecutive image frame (in this case 100 pixels). Subsequently, the logical AND function of these images was calculated. From this image, the kernel areas were calculated again and compared to the areas of the original image (Fig. 4a). If a kernel was not observed before, its area in the original and ANDed image remains constant, but if it was observed before, its area becomes smaller (Fig. 4c). This change in area was used to eliminate the kernels from the frame, and this reduced frame was then added to the shifted second image. After all kernels were selected (and counted), they were overlaid with consecutive image frames to create a kernel map where all kernels were aligned as on the original ear but represented in a linear map similar to a scroll, as shown in Fig. 5. Note that this kernel map has an existing kernel that was missed (row 5, above the second kernel from the bottom), and there are still "bridges" that need to be de-bridged (row 5, top 5 kernels, these are the broken kernels shown in Fig. 3).

2.3.3. *Kernel de-bridging*

Ideally, the kernel map as shown in Fig. 5 would consist of isolated areas (blobs) that represent single kernels. However, owing to imperfect segmentation, and in some cases, the presence of underdeveloped or broken, flat-faced kernels, some of these areas are connected to two or more other kernel areas. Figure 6 shows an example, where a central kernel is connected with adjacent kernels through two bridges. Bridged kernels can be distinguished by calculating their connected areas, which are distinct from those of non-bridged kernels and they could be compensated for. However, this only allows compensation of the kernel count: breaking up the bridges is a more elegant method, since it restores the original kernels from which other morphological parameters can be calculated. Hence, a de-bridging algorithm was applied which worked as follows. When a bridged kernel was detected based on area discrimination, the image as shown in Fig. 6a was traced back to the original grey-scale image, to allow applying the de-bridging algorithm. The de-bridging algorithm consisted of 1) extraction of the bridged area (Fig. 6a) from the kernel map, 2) retrieving the grey scale bridged area from the original ear image (Fig. 6b), 3) segmentation of the grey scale bridged area using Otsu's method with a local threshold, and

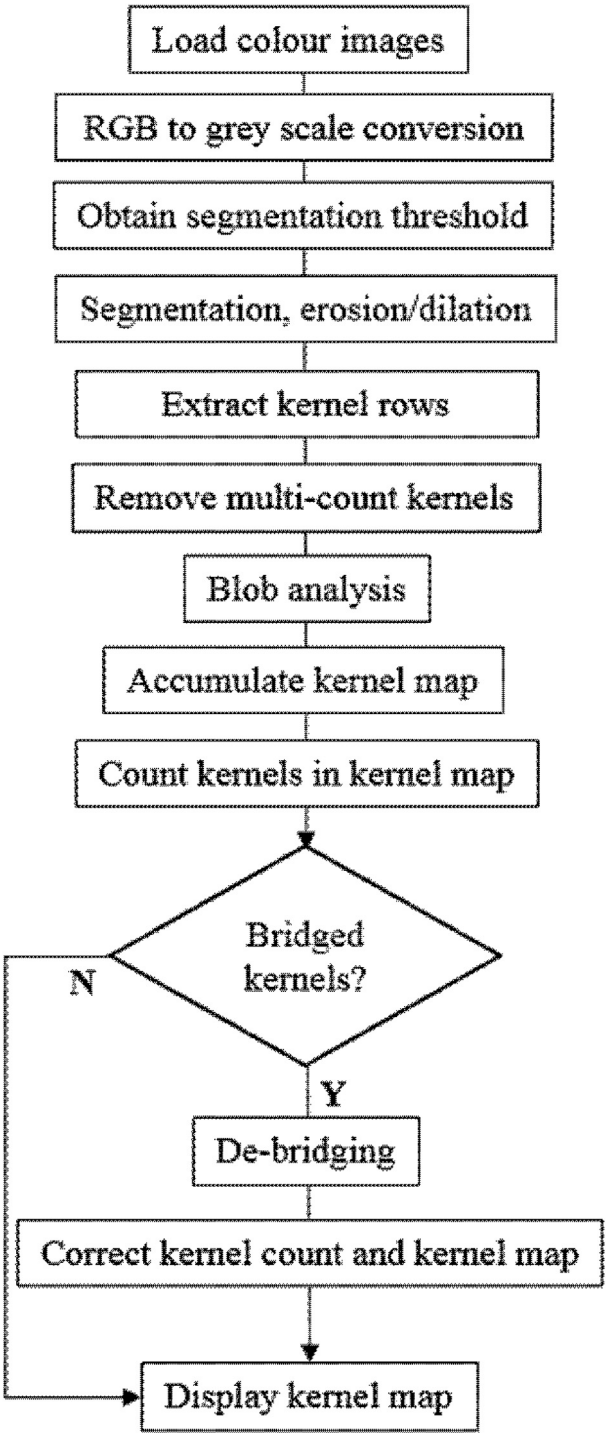

Fig. 7 – Algorithm flow chart.

Table 1 – Counting errors using total ear kernel count method.

Image	Reference ear length, D1 (pixel)	Total ear length, D2 (pixel)	Actual kernels at D1	Actual kernels at D2	Estimated kernels at D2	No. of rows	Actual total kernels at D2	Estimated total kernels at D2	Missing kernels at D2	Error (%)
1	601	865	30	44	43	14	616	604	12	1.95
2	599	737	31	38	38	14	532	534	−2	−0.38
3	683	830	32	42	39	14	588	544	44	7.48
4	610	744	31	38	38	14	532	529	3	0.56
5	566	747	30	37	40	14	518	554	−36	−6.95
6	602	749	29	37	36	14	518	505	13	2.51
7	656	800	33	44	40	14	616	563	53	8.60
8	580	729	32	41	40	14	574	563	11	1.92
9	611	778	30	39	38	14	546	535	11	2.01
10	617	771	34	43	42	14	602	595	7	1.16
11	584	749	33	43	42	14	602	593	9	1.50
12	584	748	30	40	38	16	640	615	25	3.91
13	577	749	34	41	44	14	574	618	−44	−7.67
14	653	773	35	40	41	12	480	497	−17	−3.54
15	683	839	37	45	45	14	630	636	−6	−0.95
16	683	835	37	44	45	14	616	633	−17	−2.76
17	626	770	33	40	41	14	560	568	−8	−1.43
18	615	768	34	41	42	14	574	594	−20	−3.48
19	689	828	37	43	44	12	516	534	−18	−3.49
20	569	723	31	37	39	16	592	630	−38	−6.42
21	616	749	32	38	39	16	608	623	−15	−2.47
22	610	714	32	39	37	14	546	524	22	4.03
23	588	728	31	40	38	14	560	537	23	4.11

4) writing the de-bridged area (Fig. 5c) back into the kernel map image. Note that sometimes, in the segmentation process, a hole emerged in the de-bridged binary image (Fig. 6c), but these were easily filled using MatLab's "imfill" function. Overall, the de-bridging algorithm worked well, except for underdeveloped kernels such as shown in Fig. 3, row 7, 11th kernel from the bottom. This kernel is so intimately bridged with the kernel above it, that de-bridging proved futile, therefore it was counted as a single kernel. Figure 7 shows a flow chart of all the steps in the image processing algorithm.

3. Results and discussion

The total ear kernel counting method was tested among 23 maize ears and the results are presented in Table 1. For each ear image, the length of the quasi-cylindrical mid-section (D1) in pixel and the measured length of the ear (D2) in pixel are shown, along with the manually counted actual number of kernels associated with these lengths. These factors allow for the calculation of the estimated number of kernels at D2 by multiplying the actual number of kernel at D1 by the ratio of D2 and D1. For example, for ear image 1, the estimated number of kernels at D2 was 30*865/601 = 43.178, rounded to 43 kernels in the table. To estimate the total ear kernel count, this number was multiplied by the counted number of rows, yielding 43.178*14 = 604.49, rounded to 604 kernels in the table. Finally, the error was calculated as a signed percentage by dividing the number of missing kernels at D2 by the actual total kernels at D2 as in 12/616 = 1.95%. The total ear kernel counting method was expected to be biased toward multi-counting, since the tapered base and tip were treated as if they were part of the quasi-cylindrical mid-section. However, the measurements proved this assumption incorrect, as the error percentage ranged from +8.60 to −7.67%. In the future, improvements could be made by automatically detecting the quasi-cylindrical mid-section length, although this would also include an arbitrary factor, since maize ears are only approximately cylindrical. Nevertheless, it would indeed improve the consistency of the measure, at a cost of additional computing time.

To evaluate the performance of the quasi-cylindrical mid-section kernel counting algorithm, twelve maize ears were

Fig. 8 – Colour images of twelve representative maize ear samples, ordered from simple with relatively straight kernel rows (1) to complex with helical shaped kernel rows (12).

tested ranging from simple to complex as shown from left to right in Fig. 8. Kernel maps were generated for all maize ears as shown in Fig. 9, where the top left image/map represents ear 1 and the top right image/map ear 2 and so on. The number of multi-counted kernels can be seen in the maps; if no multi-count occurred, the kernels are shown in black (this is the case for ear 6 and 7), but if a multi-count did occur, the kernels are shown in grey, and the multi-counted kernels overlaid in black. The number of multi-counted kernels for ear 1 through 12 were 1,3,3,4,3,0,0,1,3,1,1,5. Table 2 shows the errors in terms of missing kernels as well as multi-count kernels. The number of missing kernels was calculated by subtracting the number of computer counted kernels from the number of manually counted kernels. Note that the number of computer counted kernels plus the missing kernels, minus the number of multi-counted kernels does not necessarily add up to the number of manually counted kernels. This is because the computer in some cases counted only a single kernel where two manually counted kernels were present, for instance in the case of the underdeveloped kernel where the de-bridging algorithm failed. The error percentages for both the missing and multi-counted kernels were calculated by dividing the number of erroneous kernels by the manually counted kernels. The error ranged from 0 to 4.24% for missing kernels, and from 0 to 1.92% for multi-counted kernels. The maximum combined error was 5.44% with a missing error count of 4.18% and a multi-count error of 1.26%. In total, 41 kernels were missed and 25 kernels were multi-counted among 2713 computer counted kernels.

The left hand subplot of Fig. 10 shows the correlation between the manually counted number of kernels versus the machine vision estimated equivalent for the total kernel ear count method whereas the right hand subplot shows the same for the quasi-cylindrical mid-section counting method. Since these methods estimate different measures, no comparison between them is valid.

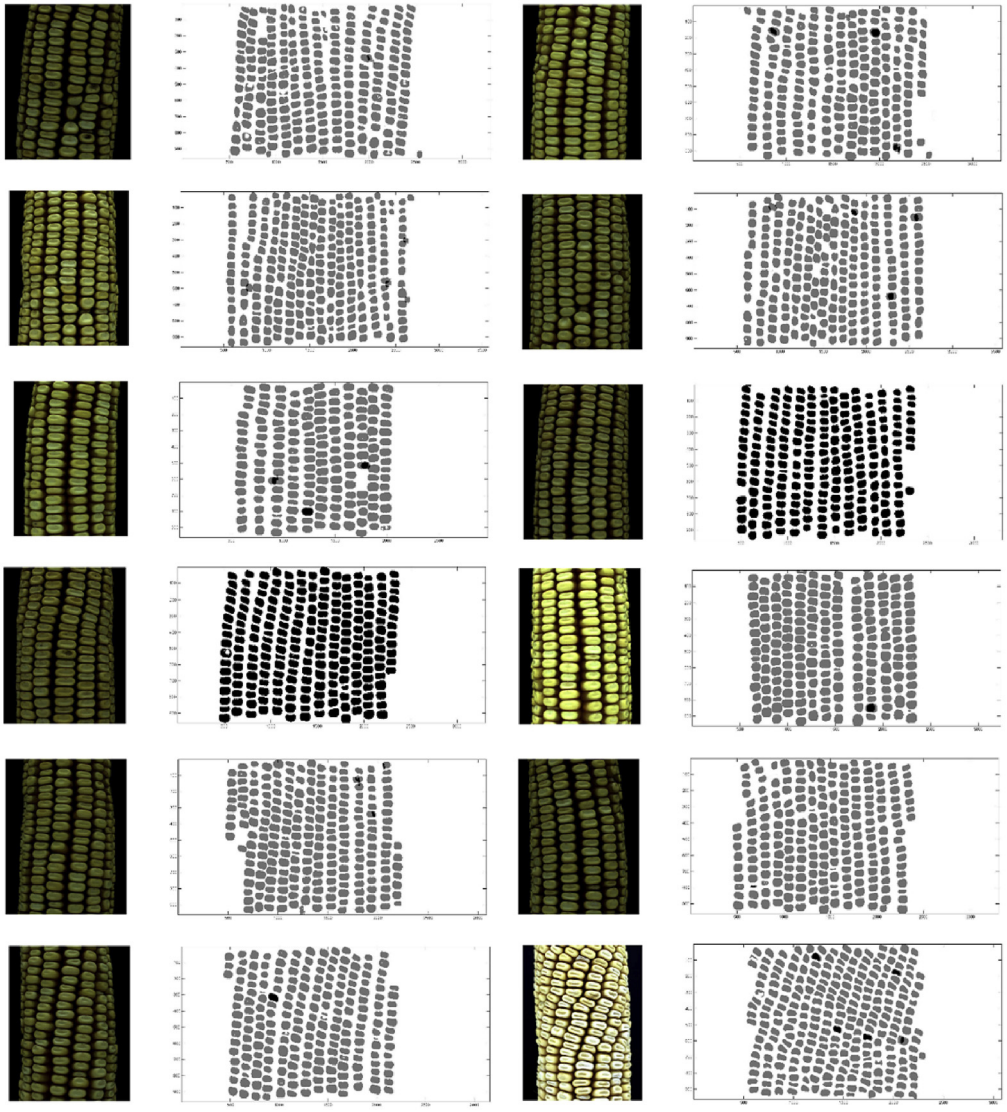

Fig. 9 – Kernel maps of all maize ears shown in Fig. 8. If no multi-counts occurred, the kernels are shown in black. In case of multi-counts, the kernels are shown in grey, and the multi-counted kernels in black.

Table 2 – Counting errors during kernel counting in the quasi-cylindrical mid-section of the ear.

Image	Missing kernels	Multi-counted kernels	Computer counted	Manually counted	Missing error (%)	Multi-count error (%)
1	3	1	235	238	1.26	0.42
2	5	3	212	217	2.30	1.38
3	0	3	265	265	0.00	1.13
4	5	4	234	239	2.09	1.67
5	2	3	172	174	1.15	1.72
6	10	0	226	236	4.24	0.00
7	6	0	229	235	2.55	0.00
8	0	1	209	209	0.00	0.48
9	10	3	229	239	4.18	1.26
10	0	1	227	227	0.00	0.44
11	0	1	215	215	0.00	0.47
12	0	5	260	260	0.00	1.92

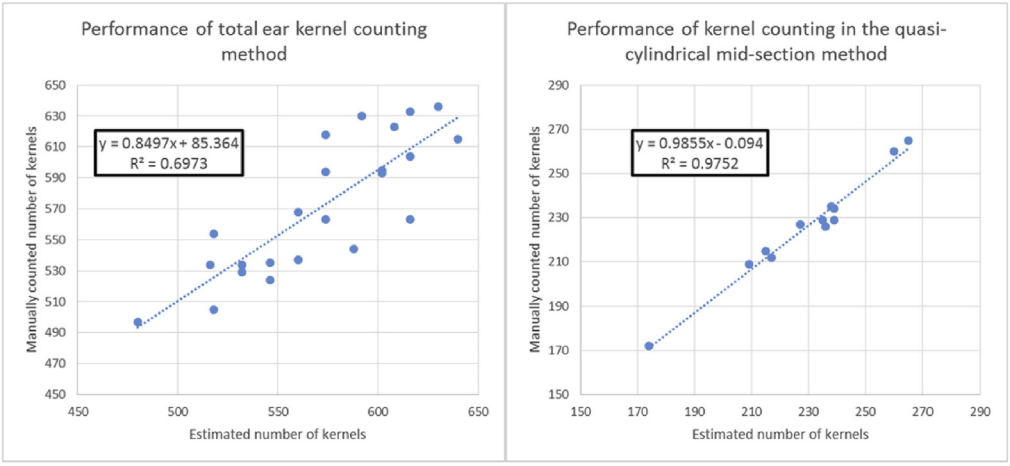

Fig. 10 – Correlation between the manually counted and machine vision estimated number of kernels for the total ear kernel counting method (left) and quasi-cylindrical mid-section method (right). No comparison between the methods is valid, since they are not alternative methods of estimating the same measure.

In the future, methods could be developed to improve the segmentation process in an attempt to eliminate bridging, such as the distance transform. In addition, higher resolution cameras would improve the overall process, at a cost of processing time. In fact, it is conceivable that, apart from feeding ears, the whole system could be automated using an industrial robot, but this would become excessively cost prohibitive.

4. Conclusions

A machine vision based method was used to predict the total ear kernel count by extrapolating the manually counted number of rows and the number of kernels in a single row located within an arbitrarily chosen quasi-cylindrical mid-section of the ear. Although the method required ample human interaction, it was simple, and achieved a kernel count error ranging from −7.67% (under-count) to +8.60% (multi-count) among 23 maize ears.

Secondly, a machine vision based approach was used to count the number of kernels in a fixed quasi-cylindrical mid-section of maize ears. This method also allows for calculation of a range of morphological parameters of individual kernels. Although precautions were taken to prevent multi-counting of kernels, it occurred 25 times among 2713 kernels counted. Similarly, although attempts were made to avoid missing kernels, it occurred 41 times, again among 2713 kernels counted. The maximum multi-count error was 1.92% and the maximum missing kernel error was 4.23%. The maximum combined error was 5.44% with a missing kernel error count of 4.18% and a multi-count error of 1.26%.

Acknowledgements

The authors appreciate the contributions to this work by former graduate student Elizabeth Bliss.

REFERENCES

Bohn, M., Novais, J., Fonseca, R., Tuberosa, R., & Grift, T. E. (2006). Genetic evaluation of root complexity in maize. *Acta*

Agronomica Hungarica, 54(3), 291–303. https://doi.org/10.1556/AAgr.54.2006.3.3.

Grift, T. E., Novais, J., & Bohn, M. (2011). High-throughput phenotyping technology for maize roots. *Biosystems Engineering*, 110(1), 40–48. https://doi.org/10.1016/j.biosystemseng.2011.06.004.

Han, Z. Z., Li, Y. Z., Zhang, J. P., & Zhao, Y. G. (2010). Counting ear rows in maize using image process method. In *ICIC 2010-3rd International Conference on Information and Computing* (Vol. 3, pp. 329–332). https://doi.org/10.1109/ICIC.2010.269.

Hausmann, N., Abadie, T., Cooper, M., Lafitte, H., & Schussler, J. (2011). *Method and system for digital image analysis of ear traits*. United States: Patent nr: 20110285844.

Ni, B., Paulsen, M. R., & Reid, J. F. (1997). Corn kernel crown shape identification using image processing. *Transactions of the ASAE*, 40(3), 833–838.

Otsu, N. (1979). A threshold selection method from gray-level histograms. *IEEE Transactions on Systems, Man, and Cybernetics*, 20(1), 62–66. https://doi.org/10.1109/TSMC.1979.4310076.

Severini, A. D., Borrás, L., & Cirilo, A. G. (2011). Counting maize kernels through digital image analysis. *Crop Science*, 51(6), 2796–2800. https://doi.org/10.2135/cropsci2011.03.0147.

Shyu, C. R., Green, J. M., Lun, D. P. K., Kazic, T., Schaeffer, M., & Coe, E. (2007). Image analysis for mapping immeasurable phenotypes in Maize. *IEEE Signal Processing Magazine*, 24(3), 115–118. https://doi.org/10.1109/MSP.2007.361609.